IEEE Access
Multidisciplinary | Rapid Review | Open Access Journal

Received March 25, 2019, accepted May 22, 2019, date of publication May 29, 2019, date of current version June 7, 2019.

Digital Object Identifier 10.1109/ACCESS.2019.2919807

Dual-Band Infrared Radiation for Rotating Missile Attitude Measurement and Interference Compensation

MIAOMIAO XU, XIONGZHU BU, WEI HAN, AND YIHAN CAO
School of Mechanical Engineering, Nanjing University of Science and Technology, Nanjing 210094, China

Corresponding author: Xiongzhu Bu (buxu105@njust.edu.cn)

This work was supported in part by the National Natural Science Foundation of China under Grant 61675097, and in part by the Postgraduate Research and Practice Innovation Program of Jiangsu Province under Grant KYCX17_0347.

ABSTRACT With the continuous development of infrared technology and its extensive usage in the military, the infrared radiation attitude measurement technology is attracting more and more attention. Aiming at the compensation requirement for complex infrared background interference during the rotating missile infrared attitude measurement, the theoretical research on the dual-band infrared rotating missile attitude measurement is carried out. The mechanism and interference characteristics of the earth infrared radiation are analyzed according to the flying missile movement characteristics. The atmosphere propagation in 3∼5–μm and 8∼14–μm infrared radiation bands are studied, and the dual-band infrared radiation attitude measurement model is established. Then, the influence of cloud infrared radiation interference on the dual-band infrared radiation sensor is analyzed, and a nighttime dual-band infrared radiation attitude measurement difference compensation algorithm is proposed to obtain the compensated attitude angle parameter. The results of the semi-physical experiments show that the compensated roll angle error is within $\pm 0.6°$ and the pitch angle error is within $\pm 1°$. The dual-band infrared radiation attitude measurement difference compensation algorithm can effectively eliminate the effects of cloud infrared radiation interference and improve the anti-interference ability of infrared radiation attitude measurement.

INDEX TERMS Dual-band, infrared radiation, attitude measurement, rotating missile, interference compensation.

I. INTRODUCTION

The infrared radiation measurement technology has become a frontier science with promising application prospects. Studies show that the infrared radiation of the sky and earth can be used for rotating missile attitude measurement [1], [2]. In the single-band infrared radiation attitude measurement, the random infrared radiation interference such as cloud layer often uses the multi-sensor mean algorithm to weaken the influence of infrared radiation background interference, which is difficult to be avoided [3]–[5]. In order to further improve the infrared attitude measurement accuracy, it is urgently to propose an infrared attitude measurement compensation method in the case of random infrared background interference by inverting the infrared radiation interference characteristics. And apply it to the rotating missile attitude angle compensation to improve the infrared radiation attitude measurement accuracy [6], [7].

At present, the infrared radiation attitude measurement is generally based on single-band. Relevant data reported that researchers in the United States use infrared sensors to conduct attitude measurement research on smart ammunition. The impact test shows that the civilian infrared sensor can withstand the impact of 12000g, and the infrared sensor can be used to measure the missile roll angle and roll rate [8], [9]. Yu Jing et al. analyzed the variation law of long-wave infrared radiance between sky and earth. Under ideal conditions, the long-wave infrared sensor measurement model was preliminarily established, and the relationship between the missile attitude angle and the infrared sensors' sensing signal was derived [10]. However, the influence of infrared radiation background interference on the

The associate editor coordinating the review of this manuscript and approving it for publication was Avishek Guha.

attitude measurement is not well considered. Studies have shown that the atmospheric scattering and absorption in the range of 3∼5μm and 8∼14μm is small, and they are ideal thermal infrared remote sensing band [11]. The mid-wave and long-wave infrared source images are decomposed into the multi-scale and multidirectional subbands by using a nonsubsampled contourlet transform(NSCT) method, and this visibility-enhanced dual-band infrared image fusion algorithm based NSCT is more suitable for human eye observation and understanding [12]. You Lu proposed a medium-wave infrared dual-band measurement method for the measurement of military target radiation characteristics, and proposed several methods to improve the measurement accuracy of dual-band radiation characteristics [13]. Yu B used Dual Band Infrared Detection (DBID) to detect the longitudinal tear of conveyor belts, not limited by dark and dusty environment [14].

Based on the usually used 8∼14μm single-band infrared radiation attitude measurement, this paper applies the dual-band infrared radiation measurement technology to the attitude measurement and navigation technology field. The combination of mid-band and long-band infrared radiation is used to detect the infrared radiation background interference. The theoretical study on the rotating missile attitude measurement with 3∼5μm and 8∼14μm infrared radiation fields is carried out. And optimizing the dual-band infrared radiation installation array. The cloud infrared radiation interference on the dual-band infrared radiation sensor is designed to eliminate the external environmental interference influence in the infrared attitude measurement and improve the infrared attitude measurement anti-interference ability.

II. DUAL-BAND THEORETICAL MODEL

A. DUAL-BAND INFRARED TRANSMITTANCE

The intensity of the radiation field in the medium is closely related to the transmittance of the medium. Therefore, it is important to study the radiation attenuation by atmosphere absorption and scattering. The atmospheric transmittance is mainly composed of two parts: the atmospheric absorption transmittance and the atmospheric scattering transmittance. In the 3∼5μm and 8∼14μm infrared band, the water vapor and carbon dioxide absorption is mainly considered. The molecule spectral absorption needs to be calculated according to the spectral line parameters or the atmospheric absorption band model, but this calculation theory is complicated and huge. The simpler method is calculating according to the existing atmospheric transmittance table. Fig. 1 shows the relationship between the water vapor and carbon dioxide transmittance in 3∼5μm and 8∼14μm infrared band and the precipitation and path length obtained from the table data provided by Liu L of Harbin Institute of Technology [15], [16].

In Fig. 1, the water vapor transmission rate curve corresponds to the precipitation amount $w_0 = 0.1, 1, 10, 100, 200, 500, 1000$mm from top to bottom, and the carbon dioxide transmission rate curve corresponds to the path length $x = 0.1, 1, 10, 100, 200, 500, 1000$km from top to bottom. As shown in Fig. 1, the water vapor and carbon dioxide content determines the infrared radiation atmospheric transmission.

The water vapor absorption transmittance can be calculated by obtaining the amount of condensable water w_0 in the transmission distance, as shown in equation (1).

$$w_0 = \rho_s \cdot RH \cdot X \tag{1}$$

In equation (1), ρ_s is the saturated water vapor density at a certain temperature, and the unit is g/m^3. It can be obtained by looking up the table according to the atmospheric temperature. RH is the relative humidity. X is the horizontal transmission distance (km).

After the sea level condensable water amount w_0 is calculated, the transmittance can be obtained by looking at the sea level water vapor spectral transmittance table, but the condensable water amount needs to be corrected when the observation point is at a certain height h, the correction is shown in equation (2).

$$w_h = \rho_s \cdot RH \cdot X \cdot e^{-a \cdot h} \tag{2}$$

In equation (2), $a = 0.0654$.

The effect of carbon dioxide on infrared transmission is calculated similarly to water vapor. After infrared radiation level transmission distance X is measured, the transmittance could be checked by horizontal carbon dioxide spectral transmittance table [17], [18]. Similarly, the carbon dioxide transmission rate also needs to be corrected with h, as shown in equation (3).

$$X_h = X \cdot e^{-b \cdot h} \tag{3}$$

In equation (3), $b = 0.313$.

When the water vapor and carbon dioxide absorption transmittance is obtained, the atmosphere absorption transmittance can be calculated according to equation (4).

$$\tau_a = \tau_{H_2O} \cdot \tau_{CO_2} \tag{4}$$

In equation (4), τ_a is atmospheric absorption transmittance, τ_{H_2O} is water vapor absorption transmittance, τ_{CO_2} is carbon dioxide absorption transmittance.

According to the sea level water vapor and carbon dioxide transmittance data in 3∼5μm and 8∼14μm infrared band, the height is corrected by equation (2) and (3), and the different wavelengths and different heights are calculated by substituting into equation (4). The atmospheric absorption transmittance curve is shown in Fig. 2.

When radiation is transmitting in the atmosphere, the radiant energy attenuated due to the molecules selective absorption, also the radiation direction changes under the gas molecules density fluctuations and tiny particles. These factors weaken the radiant energy in the propagation direction which is known as scattering attenuation. In the infrared band, sky atmospheric scattering mainly considers aerosol scattering. The scattering transmittance is generally processed

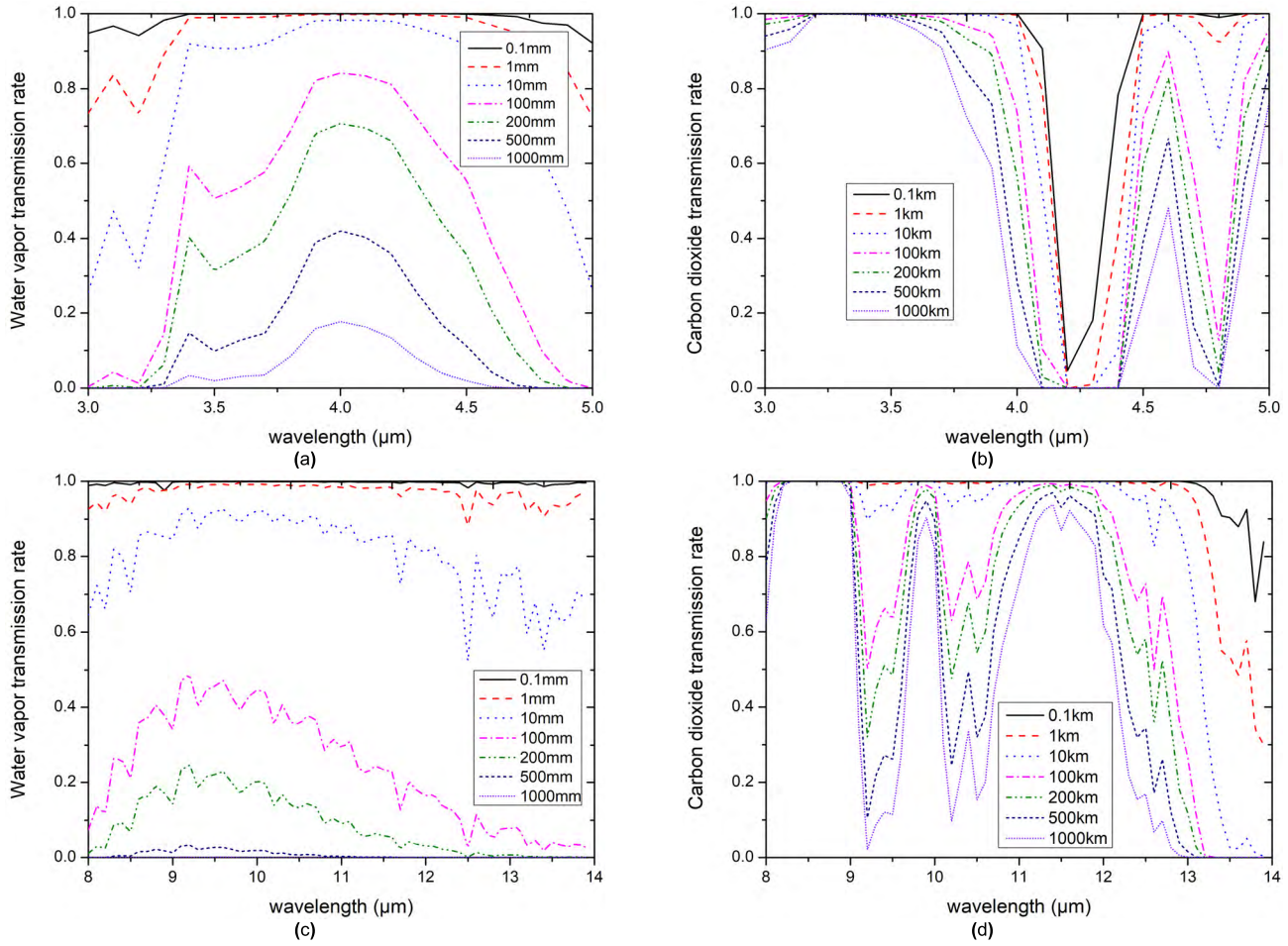

FIGURE 1. Transmission curve: (a) 3∼5μm band in water vapor; (b) 3∼5μm band in carbon dioxide; (c) 8∼14μm band in water vapor; (d) 8∼14μm band in carbon dioxide.

by the meteorological sight line in engineering, and can be calculated by equation (5).

$$\tau_{s0} = \exp[-\frac{3.91}{V}(\frac{\lambda_0}{\lambda})^q x] \tag{5}$$

In equation (5), τ_{s0} is the sea level scattering transmittance, and V is the meteorological sight line at the wavelength λ_0, usually $\lambda_0 = 0.55\mu$m. When V >80km, $q = 1.6$; when V <6km, $q = 0.585 \cdot V^{1/3}$; when V is between the two, $q = 1.3$.

The sea level atmospheric scattering transmittance can be calculated by the equation (5). The atmospheric scattering transmittance at other different heights also needs to be corrected with h. The height correction is shown as equation (6).

$$\tau_s = \tau_{s0}^{\exp(-h/h_0)} \tag{6}$$

In equation (6), h_0 generally taking 1.2km.

The sea level atmospheric scattering transmittance of is corrected by equation (6), and the atmospheric scattering transmittance at different wavelengths and heights is calculated, as shown in Fig. 3.

After the atmosphere absorption and scattering transmittance is obtained, the atmosphere total transmittance can be calculated by equation (7).

$$\tau = \tau_a \cdot \tau_s \tag{7}$$

Substitute the atmospheric absorption transmittance and scattering transmittance into equation (8), the atmospheric transmittance at different wavelengths and different heights could be calculated, as shown in Fig. 4.

B. DUAL-BAND ATTITUDE MEASUREMENT MODEL

At present, the atmospheric infrared radiation can be generally calculated by the layered theory [14]. Assuming that the observation point is located at height h. When the observation point is facing upward, the ground inclination angle in within $0 \leq \beta < \pi$. In the 3∼5μm and 8∼14μm bands atmospheric window, the infrared radiation received at the observation point is the atmospheric downward radiation. Firstly, the certain layer infrared radiation brightness at specified wavelength is calculated, and then calculate each layer's infrared radiation brightness received by the observation point with each layer's atmospheric transmittance.

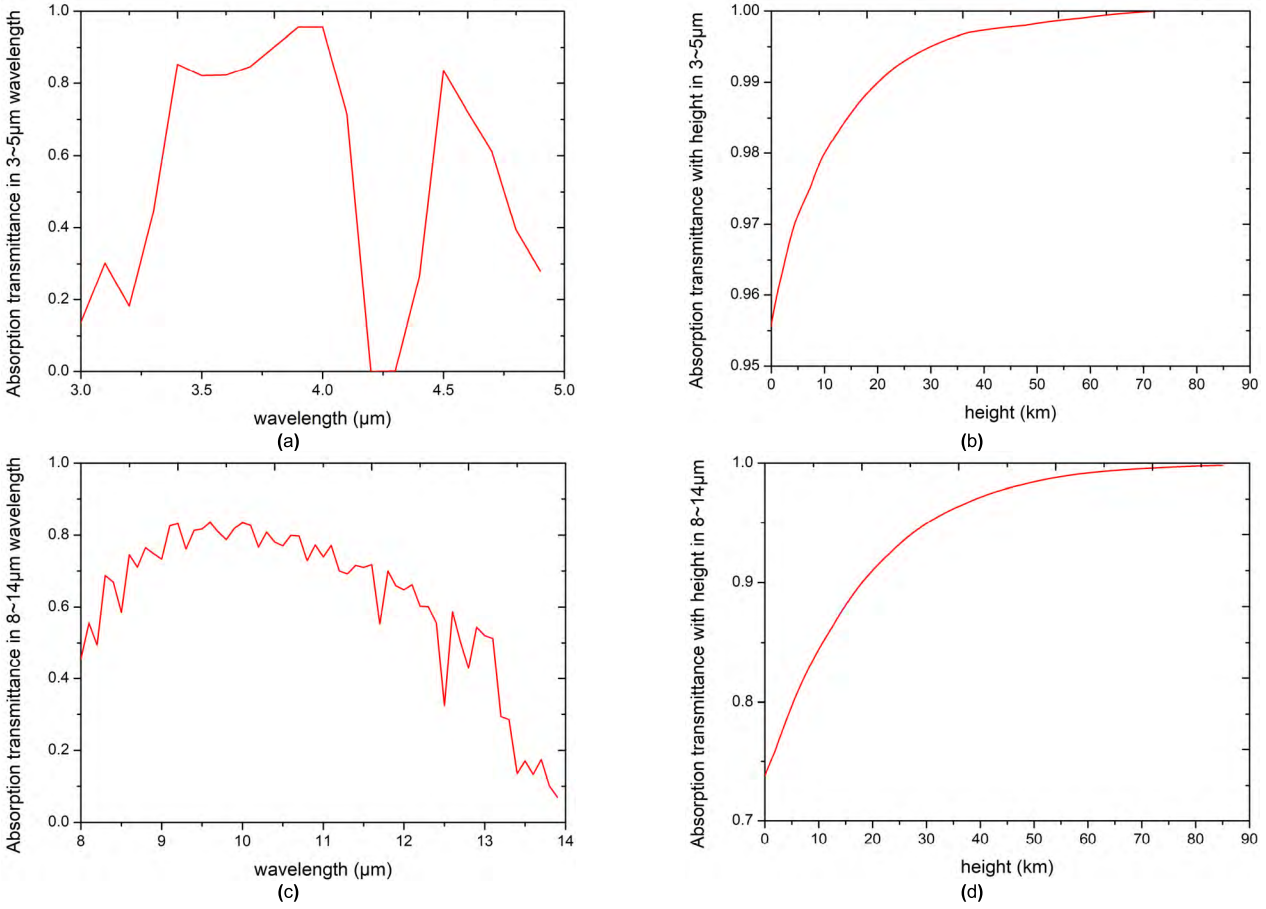

FIGURE 2. Absorption transmittance curve: (a) relationship between absorption transmittance and wavelength in 3∼5μm band; (b) relationship between absorption transmittance and height in 3∼5μm band; (c) relationship between absorption transmittance and wavelength in 8∼14μm band; (d) relationship between absorption transmittance and height in 8∼14μm band.

Then accumulate the n layer's atmosphere infrared radiation brightness. Finally, by integrating the 3∼5μm and 8∼14μm bands, the atmosphere downward infrared radiation received by the observation point can be obtained by equation (8).

$$L_{up} = \frac{1}{\pi}\int_{\lambda_1}^{\lambda_2}\sum_{i}^{n}\frac{C_1\varepsilon_{si}(\lambda,\beta)\lambda^{-5}}{\exp(C_2/\lambda T_{si})-1}\times\prod_{i+1}^{n}\tau_i(\lambda,\beta)d\lambda \tag{8}$$

In equation (8), when λ_1 is 3μm, λ_2 is 5μm; when λ_1 is 8μm, λ_2 is 14μm. C_1 is the first radiation constant; C_2 is the second radiation constant. $\varepsilon_{si}(\lambda,\beta)$ represents the layer i atmospheric infrared emissivity. T_{si} is the layer i atmosphere temperature. $\tau_i(\lambda,\beta)$represents the layer i atmospheric transmittance, $\tau_i(\lambda,\beta) = (\tau(\lambda))^{1/\cos\beta}$ [19].

When observation point is facing downward and now the ground inclination angle in within $\pi \le \beta < 2\pi$. In the 3∼5μm and 8∼14μm bands atmospheric window, the infrared radiation received by the observation point is the sum of the atmospheric up radiation and the earth surface infrared radiation. The atmospheric up radiation calculation method is similar to the atmospheric downward radiation calculation; the infrared radiation intensity of the earth surface sensed by the observation point can be obtained by calculating the earth surface infrared radiation and combining with the atmospheric transmittance. The calculation process can be obtained by equation (9).

$$\begin{aligned}L_{down} = &\frac{1}{\pi}\int_{\lambda_1}^{\lambda_2}\sum_{1}^{i}\frac{C_1\varepsilon_{si}(\lambda,\beta)\lambda^{-5}}{\exp(C_2/\lambda T_{si})-1}\times\prod_{1}^{i-1}\tau_i(\lambda,\beta)d\lambda\\ &+\frac{1}{\pi}\int_{\lambda_1}^{\lambda_2}\frac{C_1\varepsilon_{earth}(\lambda,\beta)\lambda^{-5}}{\exp(C_2/\lambda T_{earth})-1}\times\prod_{1}^{i-1}\tau_i(\lambda,\beta)d\lambda\end{aligned} \tag{9}$$

where, $\varepsilon_{earth}(\lambda,\beta)$ is the earth surface emissivity. T_{earth} is the earth surface temperature (K). When λ_1 is 3μm, λ_2 is 5μm; when λ_1 is 8μm, λ_2 is 14μm.

Based on the theoretical analysis above, the variation law of the dual-band infrared radiation with ground inclination angle $\beta \in [0, 2\pi]$ is calculated. It is assumed that the initial position of the infrared radiation sensor sensitive direction is horizontal and the counterclockwise rotation is positive. Through MATLAB simulation, the variation curve of the dual-band infrared radiation field with ground inclination angle is obtained, as shown in Fig. 5.

It can be seen from Fig. 5, when the observation direction points vertically to the sky, the infrared radiation field has the

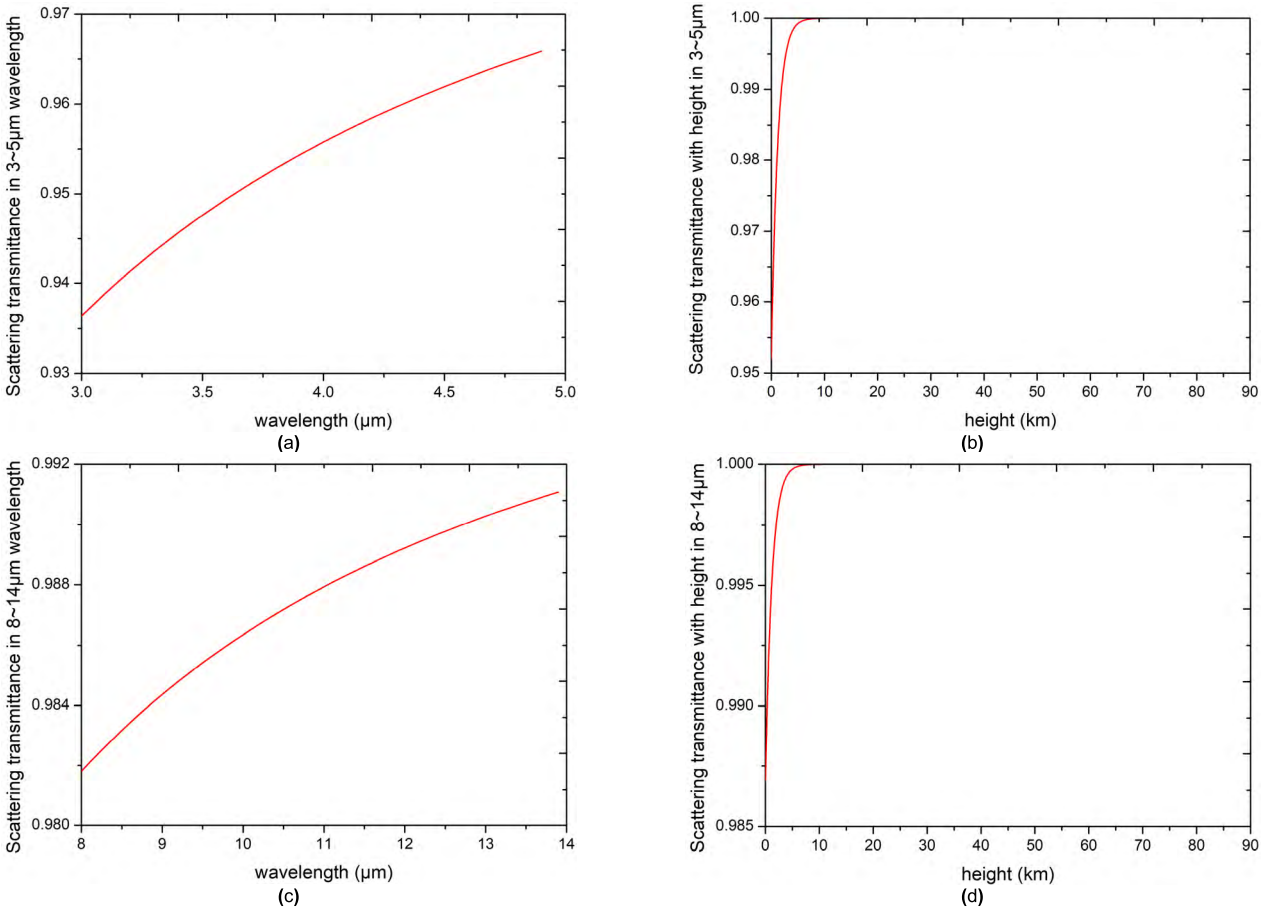

FIGURE 3. Scattering transmittance curve: (a) relationship between scattering transmittance and wavelength in 3∼5μm band; (b) relationship between scattering transmittance and height in 3∼5μm band; (c) relationship between scattering transmittance and wavelength in 8∼14μm band; (d) relationship between scattering transmittance and height in 8∼14μm band.

minimum infrared radiance in both bands. When the observation direction points vertically to the ground, the infrared radiation field has the maximum infrared radiance in both bands. Under the same background condition, the long-wave infrared radiation brightness is about 50 times higher than the medium-wave infrared radiation. Meanwhile as the ground inclination angle changes, the sky-earth infrared radiation brightness changes in a sinusoidal relationship.

Since the influence of solar light scattering isn't considered in theoretical modeling above, studies have shown that the ratio of long-wavelength solar radiation to total radiation is only 0.08% or less, and the effect in the long-wave infrared attitude measurement is almost negligible, while the mid-band solar scattered radiation is one of the main parts of total radiation, accounting for up to 80%. Therefore, the medium-wave infrared radiation attitude measurement technology can only be used when there is no solar infrared radiation at night.

III. MISSILE-BORNE DUAL-BAND INFRARED ATTITUDE MEASUREMENT METHOD

A. DUAL-BAND INFRARED SENSORS INSTALLATION

Installation of missile-borne infrared sensors requires opening windows on the missile shell. It is difficult to install infrared sensors in warhead position because of the warhead position special structure. It is necessary to open the window on the shell. The structure of the bullet position is special. It is difficult to leave space for the infrared sensor in the warhead. Therefore, it is necessary to consider a new combination of infrared sensors to avoid the impact of sensors installation on missiles performance.

It is assumed that the rotating missile mass center is at the origin point o of the missile coordinate system $o - x_b y_b z_b$, and the missile rotation axis is x_b axis and is directed to the x_b axis positive direction, as shown in Fig. 6. T_{y1} and T_{z1} are 8∼14μm infrared sensors, T_{y2} and T_{z2} are 3∼5μm infrared sensors, which are installed along the missile coordinate system y_b and z_b axes, and pointed to the positive direction.

When the rotating missile has an attitude movement in space, the missile coordinate system and the geographic coordinate system no longer coincide, and the measured value of the infrared sensors is related to the missile pitch angle θ and the roll angle γ. Through data analysis and fitting, a simplified measurement model of the missile-borne dual-band infrared sensors can be approximated as equation (10).

$$\begin{cases} V_{8\sim14}(\theta, \gamma) = A_1 \cos\theta \sin(\gamma + \delta) + B_1 \\ V_{3\sim5}(\theta, \gamma) = A_2 \cos\theta \sin(\gamma + \delta) + B_2 \end{cases} \tag{10}$$

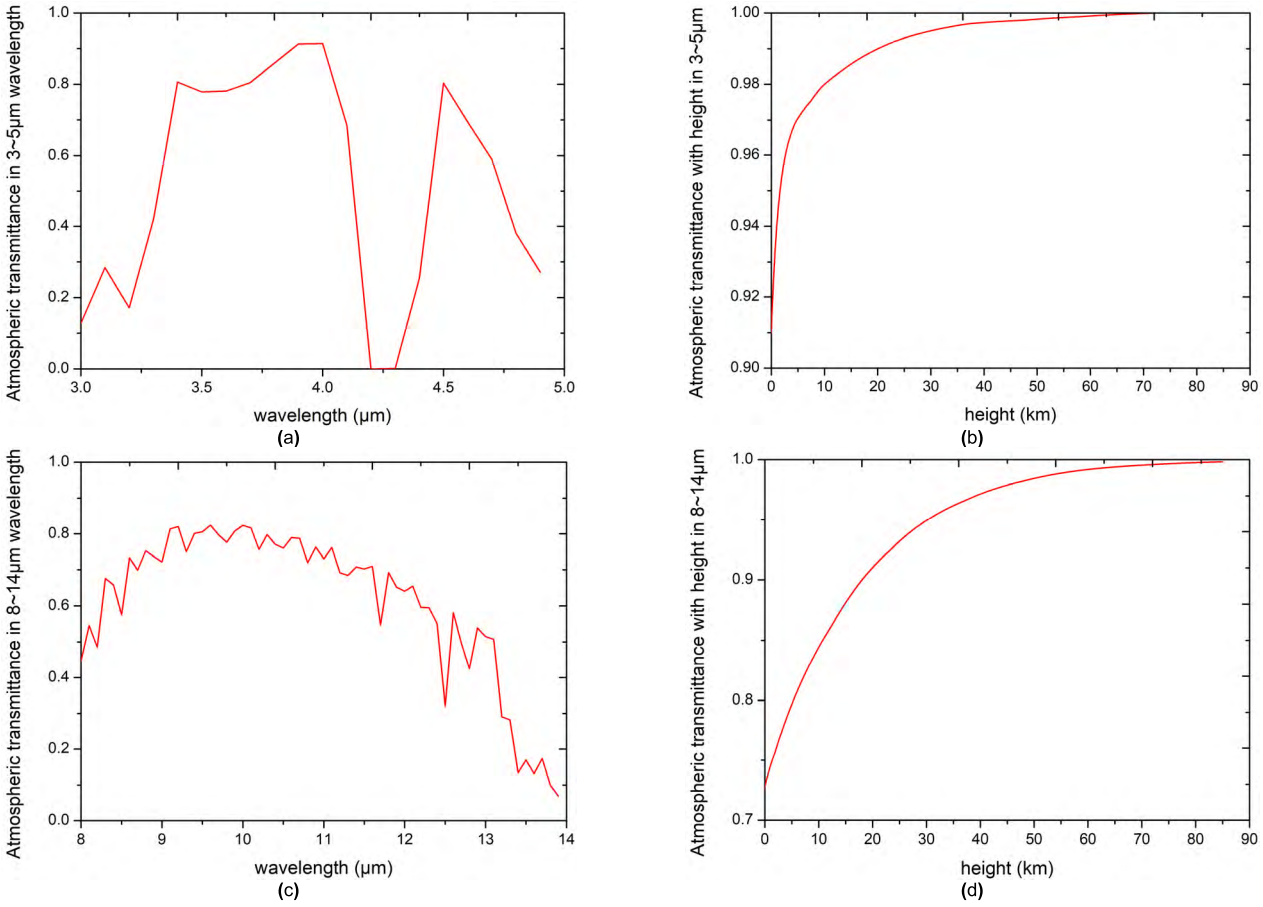

FIGURE 4. Atmospheric total transmittance curve: (a) relationship between atmospheric total transmittance and wavelength in 3∼5μm band; (b) relationship between atmospheric total transmittance and height in 3∼5μm band; (c) relationship between atmospheric total transmittance and wavelength in 8∼14μm band; (d) relationship between atmospheric total transmittance and height in 8∼14μm band.

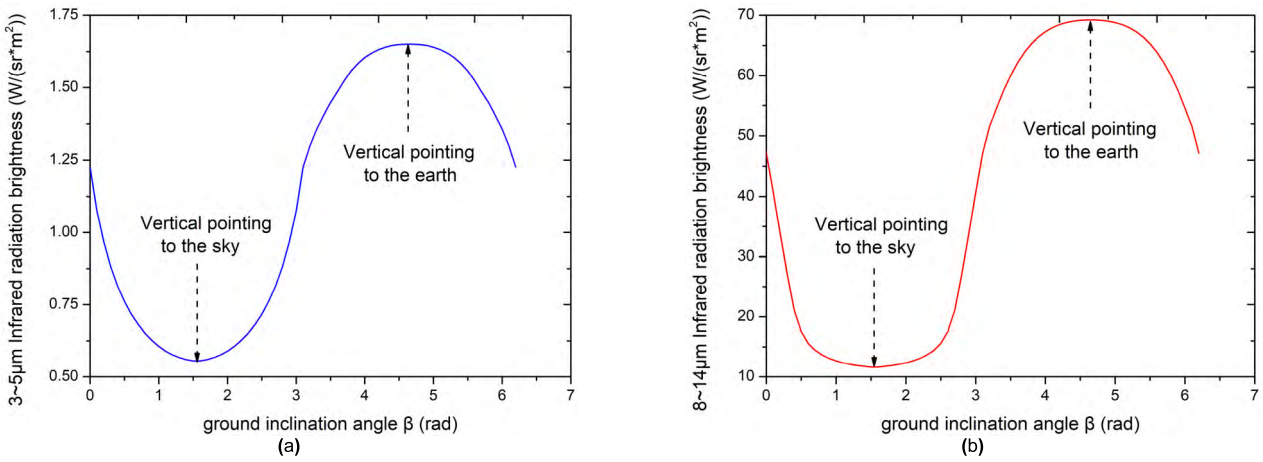

FIGURE 5. Curve of dual-band infrared radiation with ground inclination angle: (a) 3∼5μm; (b) 8∼14μm.

The two-axis dual-band infrared sensors output can be calculated according to the following equations (11) and (12) after normalizing the infrared sensor output signal amplitude A, adjusting the offset B and the phase angle δ.

$$\begin{cases} V_{y1} = \cos\theta \sin\gamma \\ V_{z1} = \cos\theta \cos\gamma \end{cases} \tag{11}$$

$$\begin{cases} V_{y2} = \cos\theta \sin\gamma \\ V_{z2} = \cos\theta \cos\gamma \end{cases} \tag{12}$$

In equations (11) and (12), V_{y1} and V_{z1} are the 8∼14μm infrared sensors output, V_{y2} and V_{z2} are the 3∼5μm infrared sensors output.

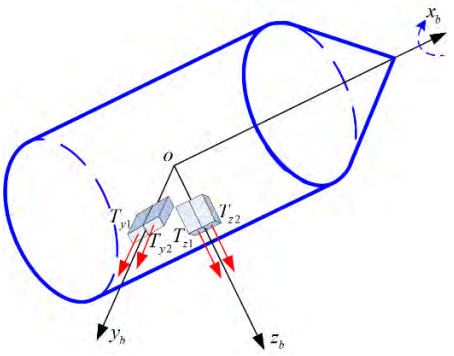

FIGURE 6. Dual-band infrared sensor installation layout diagram.

B. INFRARED ATTITUDE ANGLE DIRECT SOLUTION METHOD

The two-axis 8∼14μm infrared radiation sensors are used to demonstrate the calculation. The missile pitch angle θ range is defined in $[-90° \sim +90°]$, and the roll angle γ range is $[0° \sim 360°]$. The missile roll angle is calculated by the ratio of V_{y1} and V_{z1}, then the missile pitch angle can be calculated by combining the calculated roll angle with V_{y1} or V_{z1}.

The roll angle can be calculated according to equations (13) and (14) as below.

$$\gamma_{cal} = \arctan(V_{y1}/V_{z1}) \tag{13}$$
$$\gamma_{cal} = 90° - \arctan(V_{z1}/V_{y1}) \tag{14}$$

The pitch angle can be calculated according to equations (15) and (16) as below.

$$\theta_{cal} = \arccos(V_{y1}/\sin\gamma_{cal}) \tag{15}$$
$$\theta_{cal} = \arccos(V_{z1}/\cos\gamma_{cal}) \tag{16}$$

However, the output of V_{y1} and V_{z1} has errors in actual measurement, and the roll angle calculation is related to them. The function error transfer principle must be reasonably considered to minimize the solution result error [20].

The equations (13) and (14) standard deviations can be expressed as equations (17) and (18):

$$\sigma_{\gamma_{cal1}} = \sqrt{\frac{1}{(V_{z1})^2+(V_{y1})^2}\sigma_{V_{y1}}^2 + \frac{(V_{y1})^2}{(V_{z1})^2+(V_{y1})^2}\sigma_{V_{z1}}^2} \tag{17}$$

$$\sigma_{\gamma_{cal2}} = \sqrt{\frac{(V_{z1})^2}{(V_{z1})^2+(V_{y1})^2}\sigma_{V_{y1}}^2 + \frac{1}{(V_{z1})^2+(V_{y1})^2}\sigma_{V_{z1}}^2} \tag{18}$$

It can be known from equations (17) and (18), when $|V_{y1}| \geq |V_{z1}|$, $\sigma_{\gamma_{cal1}} \geq \sigma_{\gamma_{cal2}}$. When $|V_{y1}| < |V_{z1}|$, $\sigma_{\gamma_{cal1}} < \sigma_{\gamma_{cal2}}$. Therefore, when $|V_{z1}| \geq |V_{y1}|$, $\arctan(V_{y1}/V_{z1})$ is used to solve the roll angle. When $|V_{z1}| < |V_{y1}|$, $\arctan(V_{z1}/V_{y1})$ is used to solve the roll angle. The roll angle solution true value is shown in Table 1.

The pitch angle can be solved by using V_{y1} or V_{z1} and the calculated roll angle γ_{cal}. Therefore, it is necessary to minimize the V_{y1} and V_{z1} error transfer coefficients.

TABLE 1. Roll angle calculation truth value.

Judgment basis		roll angle γ_{cal}
$V_{y1} \geq 0$	$V_{z1} > 0$ 且 $\lvert V_{z1}\rvert \geq \lvert V_{y1}\rvert$	$\arctan(V_{y1}/V_{z1})$
$V_{y1} < 0$		$\arctan(V_{y1}/V_{z1})+360°$
$V_{y1} > 0$	$V_{z1} \geq 0$ 且 $\lvert V_{z1}\rvert < \lvert V_{y1}\rvert$	$90°-\arctan(V_{z1}/V_{y1})$
$V_{y1} < 0$		$270°-\arctan(V_{z1}/V_{y1})$
$V_{y1} \geq 0$	$V_{z1} < 0$ 且 $\lvert V_{z1}\rvert \geq \lvert V_{y1}\rvert$	$\arctan(V_{y1}/V_{z1})+180°$
$V_{y1} < 0$		
$V_{y1} > 0$	$V_{z1} < 0$ 且 $\lvert V_{z1}\rvert < \lvert V_{y1}\rvert$	$90°-\arctan(V_{z1}/V_{y1})$
$V_{y1} < 0$		$270°-\arctan(V_{z1}/V_{y1})$

TABLE 2. Pitch angle calculation truth value.

Judgment basis	Pitch angle θ_{cal}
$\lvert V_{z1}\rvert \geq \lvert V_{y1}\rvert$	$\arccos(V_{z1}/\cos\gamma)$
$\lvert V_{z1}\rvert < \lvert V_{y1}\rvert$	$\arccos(V_{y1}/\sin\gamma)$

The equations (15) and (16) standard deviations can be expressed as equations (19) and (20).

$$\sigma_{\theta_{cal}} = \sqrt{(\frac{\partial f}{\partial V_{y1}})^2\sigma_{V_{y1}}^2 + (\frac{\partial f}{\partial \gamma_{cal}})^2\sigma_{\gamma_{cal}}^2} \tag{19}$$

$$\sigma_{\theta_{cal}} = \sqrt{(\frac{\partial f}{\partial V_{z1}})^2\sigma_{V_{y1}}^2 + (\frac{\partial f}{\partial \gamma_{cal}})^2\sigma_{\gamma_{cal}}^2} \tag{20}$$

Find V_{y1} and V_{z1} partial derivatives, as shown in equation (21) and (22).

$$\left|\frac{\partial f}{\partial V_{y1}}\right| = \frac{1}{\sin\gamma_{cal}\sqrt{1-\left(V_{y1}/\sin\gamma_{cal}\right)^2}} \tag{21}$$

$$\left|\frac{\partial f}{\partial V_{z1}}\right| = \frac{1}{\cos\gamma_{cal}\sqrt{1-\left(V_{z1}/\cos\gamma_{cal}\right)^2}} \tag{22}$$

It can be known from equations (21) and (22), when the $|\sin\gamma_{cal}|$ value is larger, the $\left|\partial f/\partial V_{y1}\right|$ error transfer coefficient is smaller; when the $\cos\gamma_{cal}$ value is larger, the $\left|\partial f/\partial V_{z1}\right|$ error transfer coefficient is smaller.

Because $V_{y1} = \cos\theta\sin\gamma$ and $V_{z1} = \cos\theta\cos\gamma$, $|V_{z1}|$ and $|V_{y1}|$ can be directly compared in the actual solution process. When $|V_{z1}| \geq |V_{y1}|$, use V_{z1} to solve θ_{cal}; when $|V_{z1}| < |V_{y1}|$, use V_{y1} to solve θ_{cal}. The pitch angle solution true value is shown in Table 2.

C. NUMERICAL SIMULATION

In order to verify the attitude calculation accuracy of the two-axis infrared sensor installation method. MATLAB is used for simulation analysis. The pitch angle θ is varied within 25 to 50 degrees, and the roll angle is continuously changed in the positive direction. Random white noise with zero mean and 10^{-3}G root mean square is added [21]. Finally, the missile's

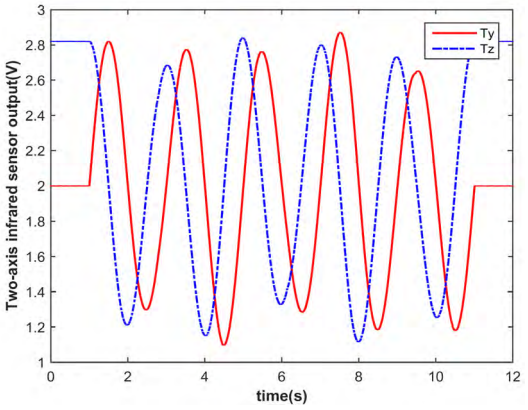

FIGURE 7. Biaxial infrared sensors output curve.

biaxial infrared sensors output curve under simulated conditions is obtained, as shown in Fig. 7.

The two-axis infrared sensor direct solution algorithm and the three-axis infrared sensor calculation algorithm [19] are used to solve the attitude angle. The solution result is shown in Fig. 8. The numerical simulation results show that the two-axis and three-axis solving algorithms have their own advantages and disadvantages.

It can be seen from Fig. 8 that the pitch angle error obtained by the three-axis calculation algorithm is smaller than the pitch angle error of the two-axis direct solution algorithm. The roll angle error obtained by the two-axis direct solution algorithm is smaller than the roll angle error of the three-axis calculation algorithm. Both algorithms can keep the pitch angle and roll angle error within $\pm 0.5°$. However, the two-axis infrared sensor simplifies the sensor installation and saves the space occupied by the infrared sensor conditioning circuit. Compared with the three-axis infrared sensor installation method, the two-axis infrared sensor installation method is relatively more reasonable.

IV. DUAL-BAND DIFFERENCE COMPENSATION

A. SIMULATION ANALYSIS OF DUAL-BAND CLOUDS INFRARED RADIATION INTERFERENCE

By referring to the analysis of the cloud layer infrared radiation interference in literature [3], the infrared attitude measurement error caused by the cloud layer infrared radiation interference on the dual-band infrared sensors output signal is studied [22]. The output of the missile-borne dual-band infrared sensor under the cloud interference influence is calculated by MATLAB, and compared with the infrared sensor output under cloudless conditions. The dual-band infrared radiation interference curve is shown in Fig. 9.

According to the results in Fig. 9, when the cloud layer enters the infrared sensor view angle, the infrared sensor output will be larger than normal conditions, since the cloud layer infrared radiance is higher than the sky; when the cloud layer leaves the infrared sensor view angle, the infrared sensor output returns to normal. By comparing the dual-band infrared sensor output, it can be seen that the cloud infrared radiation interference has little effect on the medium-wave infrared sensor output under the same cloud interference.

The dual-band attitude angle solution error under cloud interference is calculated separately, as shown in Fig. 10. It can be seen that the cloud layer has a great influence on the long-wave infrared attitude measurement accuracy. The maximum long-wave infrared radiation attitude angle error can reach 20°, while the maximum medium-wave infrared radiation attitude angle error is only 3°. By comparing with the long-wave infrared radiation, the cloud layer influence on medium-wave infrared radiation attitude measurement is small.

B. DUAL-BAND INFRARED RADIATION DIFFERENCE CALCULATION

During the missile flight, the cloud layer orientation randomly happens. The cloud layer different influence on the

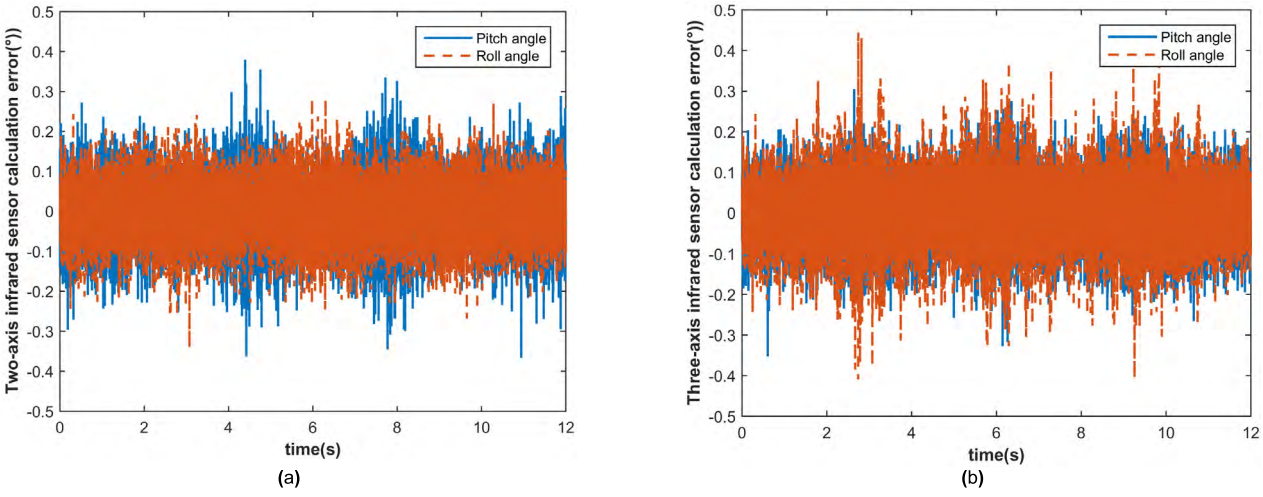

FIGURE 8. Attitude angle solution error. (a) Biaxial. (b) Triaxial.

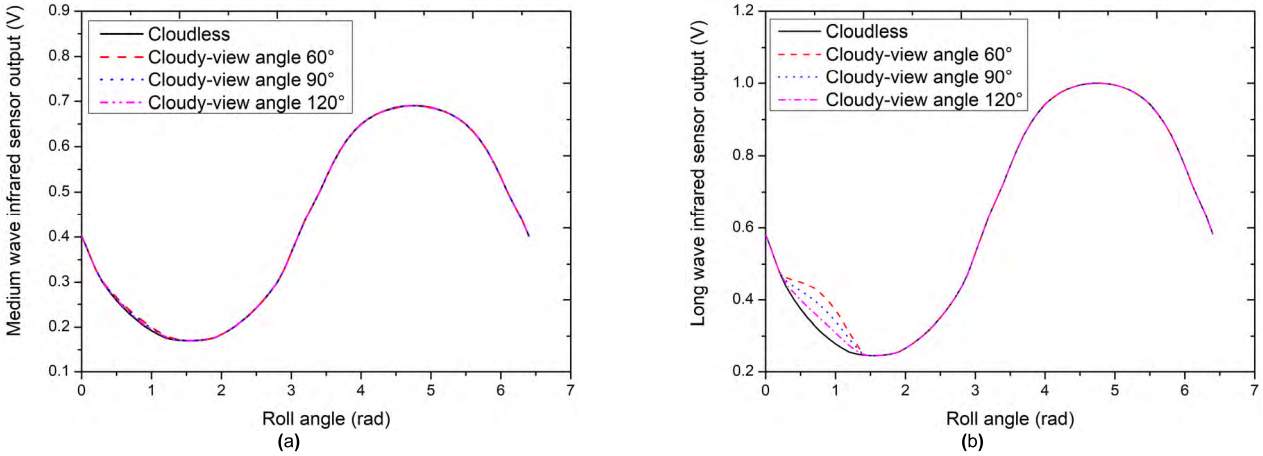

FIGURE 9. Dual-band infrared radiation curve under cloud interference: (a) 3∼5μm; (b) 8∼14μm.

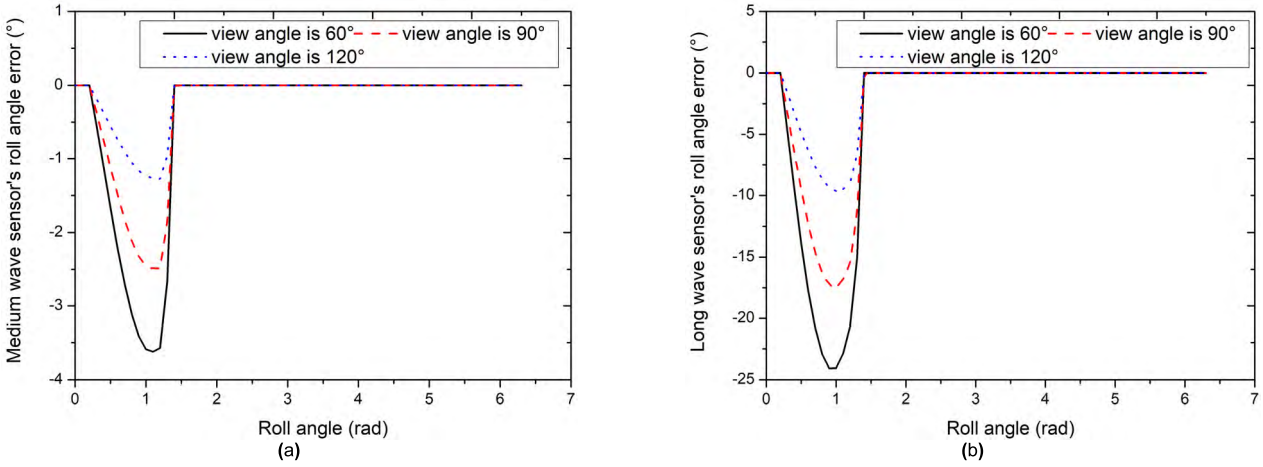

FIGURE 10. Attitude angle solution error: (a) 3∼5μm; (b) 8∼14μm.

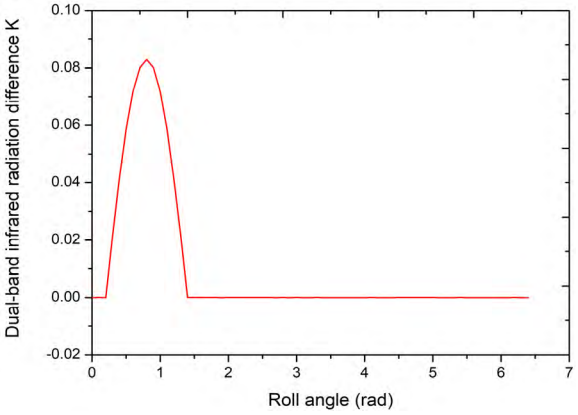

FIGURE 11. Dual-wave infrared radiation sensor difference value affected by clouds.

medium-wave and long-wave infrared radiation can be used to judge the cloud layer orientation. Then the cloud infrared radiation theoretical model is used to compensate, thereby eliminating the cloud layer infrared radiation interference.

Firstly, normalize the output of the dual-band infrared sensor, then calculate the difference between the coaxial dual-band infrared radiation sensors, and the double-band infrared radiation difference calculation equation (23) is established. The cloud layer infrared radiation location can be judged by the difference K.

$$K = V_1 - V_2 \tag{23}$$

Using the above simulation results of the long wave and the medium wave cloud layer infrared radiation interference curve, the sensor field view angle is selected as 120° to calculate the difference K, as shown in Fig. 11.

It can be seen from Fig. 11 that during the rotation of the sensor, the K value is close to 0 in the case of cloudless infrared radiation interference; when the sensor sensitive direction is gradually approaching the center of the cloud, the K value is gradually increased; when the sensor sensitive direction is facing the cloud layer, the K value reaches the maximum at the center position; when the sensor sensitive direction gradually moves away from the cloud layer center,

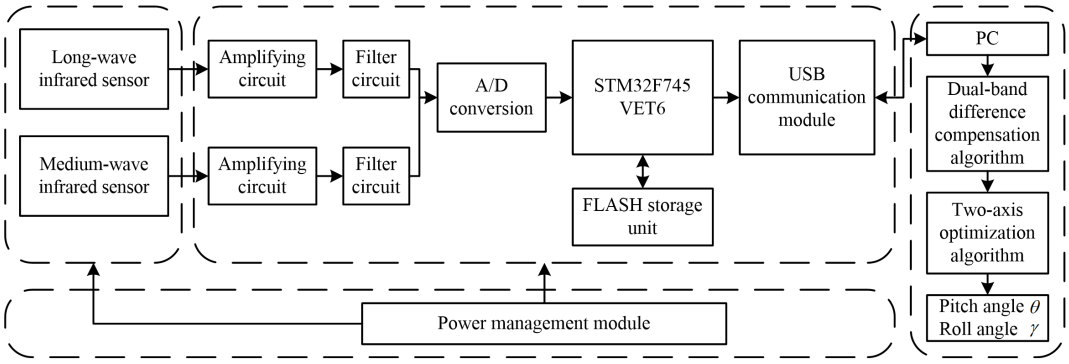

FIGURE 12. Block diagram of dual-band infrared radiation attitude measurement system.

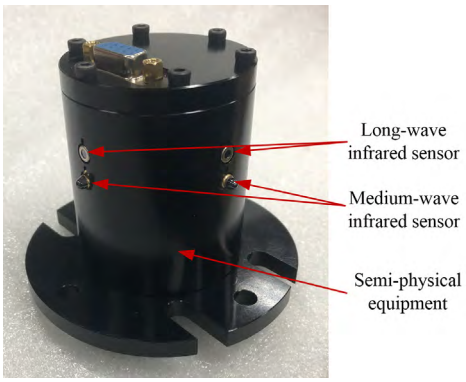

FIGURE 13. Semi-physical experiment device.

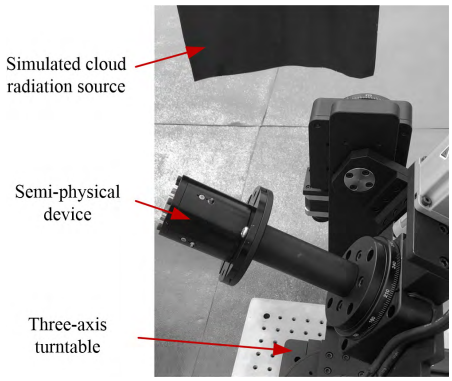

FIGURE 14. Semi-physical experiment physical picture.

the K value gradually decreases to zero. Therefore, the K value can be used to judge the time when the cloud infrared radiation interference exists, and the cloud infrared radiation can be compensated in real time.

If $K > 0$, it is considered that there is cloud infrared radiation interference at this moment, and then the value of K is used to compensate the cloud layer infrared radiation, as shown in equation (24).

$$\boldsymbol{T} = \begin{bmatrix} V_{y1} & V_{z1} \end{bmatrix}^T - \begin{bmatrix} K_y & K_z \end{bmatrix}^T \tag{24}$$

If $K = 0$, it is considered that there is no cloud infrared radiation interference, and the missile attitude can be directly calculated, as shown in equation (25). $\boldsymbol{T}$ is the output matrix after dual-band infrared radiation compensation, which is used for final attitude calculation.

$$\boldsymbol{T} = \begin{bmatrix} V_{y1} & V_{z1} \end{bmatrix}^T \tag{25}$$

V. SEMI-PHYSICAL EXPERIMENT AND DISCUSSION

The overall dual-band infrared attitude measurement circuit hardware structure is shown in Fig. 12. In the measurement system, Heimann HMS J11 F5.5 is used to measure long-wave infrared radiation, and LMS NT LMS43PD-03-CG is used to measure medium-wave infrared radiation. The dual-band infrared radiation sensors output signal is amplified and filtered by regulating circuit. STMicroelectronics' STM32F745VET6 is used as logic control core. Analog Devices' AD7606 is used as signal conversion unit. Winbond's W25Q256 is used as data storage unit. Finally, the data acquisition and storage module for the dual-band infrared attitude measurement system is designed. The module has 16-bit 8-channel simultaneous sampling, each channel has 200KSPS throughput rate, non-volatile 64MB storage depth, adjustable sampling rate, easy interaction and so on features. It can be used for signal acquisition in harsh environments such as high vibration and strong magnetism during missile flight. The above circuit devices are combined into a semi-physical experiment device, as shown in Fig. 13.

In order to verify the effectiveness of the dual-band infrared attitude measurement and cloud interference compensation algorithm, the semi-physical device is installed on a three-axis turntable, as shown in Fig. 14.

Controlling the three-axis turntable to keep the pitch and yaw angles constant, and the roll angle continuously changes. The infrared radiation source coated with black paint is used to simulate the cloud interference. It appears in the roll direction of the semi-physical device. Then the two-axis dual-band infrared sensors output is used to solve the missile attitude angle.

In the presence of cloud interference, the long-wave infrared sensor and the dual-band infrared sensor are

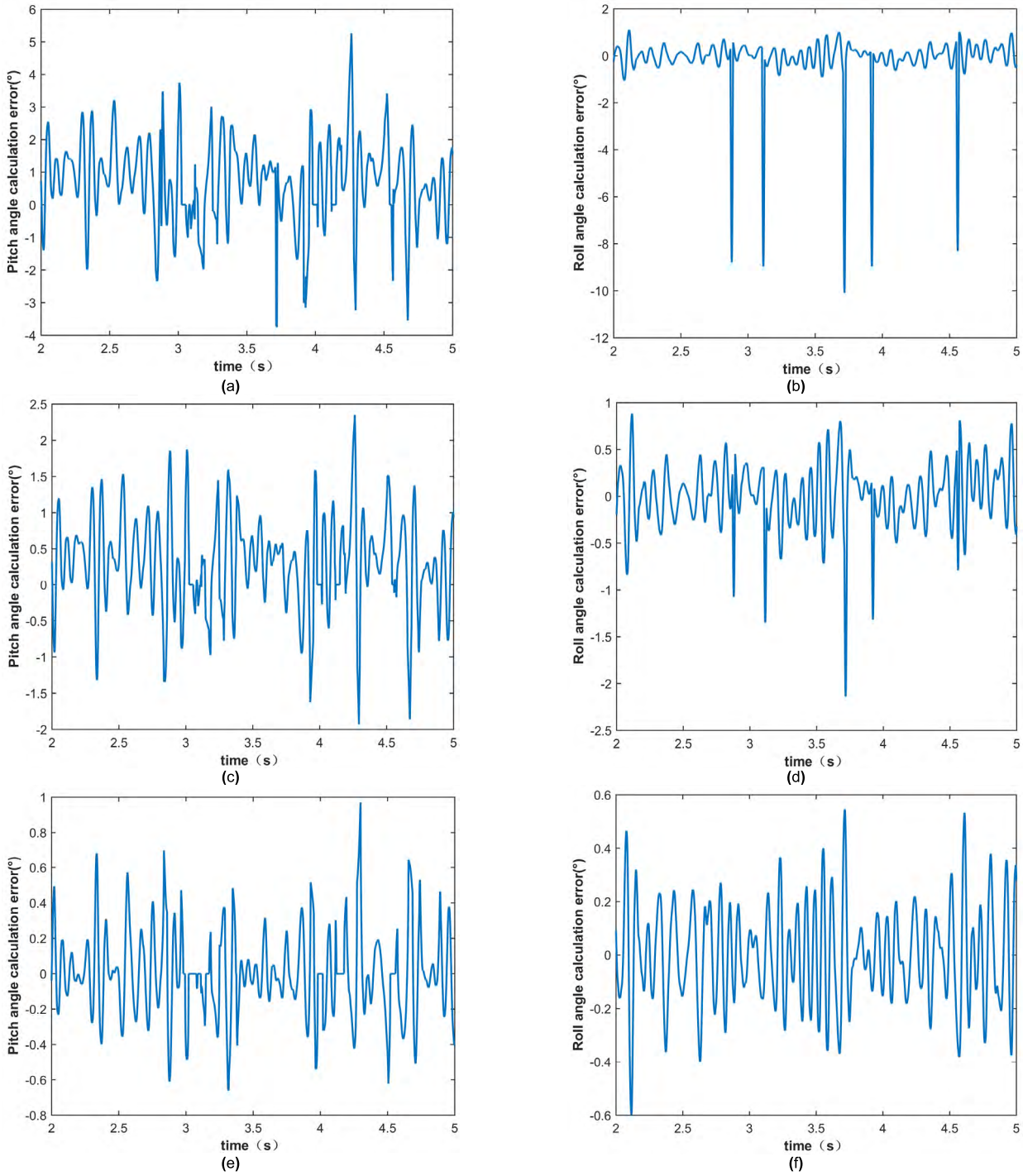

FIGURE 15. Attitude angle error under cloud interference obtained by three algorithms: (a) pitch angle error under single band direct solution algorithm; (b) roll angle error under single band direct solution algorithm; (c) pitch angle error under single band weighted fusion algorithm; (d) roll angle error under single band weighted fusion algorithm; (e) Pitch angle error under dual-band difference compensation algorithm; (f) Roll angle error under dual-band difference compensation algorithm.

respectively used to solve the missile attitude angle. The long-wave infrared sensor data is solved by direct solution method and weighted fusion algorithm. The dual-band infrared sensor data is solved by dual-wave difference compensation algorithm. In the case of simulating cloud interference, the attitude angle error of the three attitude solving algorithms is shown in Fig. 15.

It can be seen from Fig. 15 that in the case of cloud interference, the attitude angle calculation accuracy of the single-band weighted fusion algorithm is higher than single

TABLE 3. Comparison of attitude angle error.

Algorithm	Pitch angle error	Roll angle error
Single band direct solution algorithm	±5°	±12°
Single band weighted fusion algorithm	±2.5°	±3°
Dual-band difference compensation algorithm	±1°	±0.6°

band direct solution algorithm. The cloud interference cannot be completely eliminated. However, the dual-band difference compensation algorithm designed in this paper completely eliminates the cloud layer infrared radiation influence. The roll angle calculation error is within ±0.6°, and the pitch angle calculation error is within ±1°. The solution results are shown in Table 3. It is shown that the dual-band infrared radiation difference compensation algorithm can further improve the anti-cloud ability of the infrared attitude measurement system. Compared with other attitude measurement techniques, it has the advantages of high accuracy, strong anti-interference ability, without drift and cumulative error, no need for initial alignment, etc.

VI. CONCLUSION

In this study, a dual-band infrared radiation attitude measurement method is proposed to improve the anti-interference ability of infrared attitude measurement. Dual-band infrared radiation theoretical model is established. The attitude calculation algorithm with missile-born two-axis infrared radiation sensors is designed based on the error transfer theory. In order to suppress the cloud layer infrared radiation interference, a dual-band difference compensation algorithm is designed. The semi-physical experiment is used to compare the attitude calculation error of the single-band and dual-band attitude solving algorithm. The result shows that the dual-band infrared radiation difference compensation algorithm can effectively improves the anti-interference ability of infrared radiation attitude measurement. However, the dual-band infrared radiation difference compensation algorithm proposed in this paper can only work at night. The future work need to focus on selecting other bands to avoid solar infrared radiation, in order to further improve the anti-interference ability of daytime infrared attitude measurement.

REFERENCES

[1] A. G. U. Perera, G. Ariyawansa, M. B. M. Rinzan, M. Stevens, M. Alevli, N. Dietz, S. G. Matsik, A. Asghar, J. T. Ferguson, H. Luo, A. Bezinger, and H. C. Liu, "Performance improvements of ultraviolet/infrared dual-band detectors," *Infr. Phys. Technol.*, vol. 50, nos. 2–3, pp. 142–148, 2007.

[2] T. D. Nguyen, J. O. Kim, Y. H. Kim, E. T. Kim, Q. L. Nguye, and S. J. Lee, "Dual-color short-wavelength infrared photodetector based on InGaAsSb/GaSb heterostructure," *AIP Adv.*, vol. 8, no. 2, 2018, Art. no. 025015.

[3] M. Xu, X. Bu, J. Yu, and Z. He, "Compensation method of cloud infrared radiation interference based on a spinning projectile's attitude measurement," *J. Appl. Remote Sens.*, vol. 12, no. 1, 2018, Art. no. 016031.

[4] Q. Fu and K. N. Liou, " Parameterization of the radiative properties of cirrus clouds," *J. Atmos. Sci.*. vol. 50, no. 13, pp. 2008–2025, 1993.

[5] Y. Yang, H. S. Wu, and L. C. Li, "The effect of complex background infrared radiation on target scattering radiance," in *Proc. 9th Int. Symp. Antennas, Propag. EM Theory*, Dec. 2010, p. 749- 752.

[6] C. Guo, H. Cai, and G. H. M. van der Heijden, "Feature extraction and geomagnetic matching," *J. Navigat.*, vol. 66, no. 6, pp. 799–811, 2013.

[7] X. Kong, L. Liu, Y. Qian, and M. Cui, "Automatic detection of sea-sky horizon line and small targets in maritime infrared imagery," *Infr. Phys. Technol.*, vol. 76, pp. 185–199, May 2016.

[8] J. Rogers, M. Costello, and D. Hepner, "Roll orientation estimator for smart projectiles using thermopile sensors," *J. Guid. Control Dyn.*, vol. 34, no. 3, pp. 688–697, 2011.

[9] M. Don, D. Grzybowski, and I. V. Christian, *Roll Angle Estimation Using Thermopiles for A Flight Controlled Mortar*. Adelphi, MD, USA: Army Research Laboratory, 2012, pp. 1–20.

[10] Y. Jing, B. Xiong-Zhu, N. Jie, and W. Xin-Zheng, "Attitude estimator for spinning aircraft using earth infrared radiation field," *ACTA Phys. Sinica*, vol. 65, no. 7, p. 079501, Apr. 2016.

[11] P. Y. Delaunay, "Dual-band infrared detector and method of detecting multiple bands of infrared radiation," U.S. Patent 9 755 091 B2, May 9, 2017.

[12] Z. Li, J. Zhou, and Y. Wang, "Visibility-enhanced dual-band infrared image fusion based on nonsubsampled contourlet transform," *Proc. SPIE*, vol. 10462, p. 104621F, 2017.

[13] Y. Lü, X. He, Z.-H. Wei, Z.-Y. Sun, and S.-T. Chang, "Ambient temperature-independent dual-band mid-infrared radiation thermometry," *Appl. Opt.*, vol. 55, no. 9, pp. 2169–2174, 2016.

[14] B. Yu, T. Qiao, H. Zhang, and G. Yan, "Dual band infrared detection method based on mid-infrared and long infrared vision for conveyor belts longitudinal tear," *Measurement*, vol. 120, pp. 140–149, May 2018.

[15] L. Liu, S. Dong, and Q. Yu, "Atmospheric mean transmittance in wavelength interval 0.1μm from infrared 1 to 14μm, (I) transmittance of carbon dioxide," *J. Harbin Inst. Technol.*, vol. 30, no. 5, pp. 8–12, 1998.

[16] L. Liu, S. Dong, and Q. Yu, "Atmospheric mean transmittance in wavelength interval 0.1μm from infrared 1 to 14μm, (II)transmittance of water vapor," *J. Harbin Inst. Technol.*, vol. 31, no. 6, pp. 75–78, 1999.

[17] A. Berk and C. Rice, "Modtran6 Multiple Line-Of-Sight (MLOS) Option," in *Proc. IEEE Int. Geosci. Remote Sens. Symp.*, Jul. 2018, pp. 1703–1706.

[18] X. Y. Li, C. L. Ma, and W. Zhi, "Design of attitude measurement system for UAV based on infrared sensing principle," *Transducer Microsyst. Technol.*, vol. 33, no. 9, pp. 101–103, 2014.

[19] M. Xu, X. Bu, J. Yu, and Z. He, "Spinning projectile's attitude measurement with LW infrared radiation under sea-sky background," *Infr. Phys. Technol.*, vol. 90, pp. 214–220, May 2018.

[20] S. Park, M.-S. Gil, H. Im, and Y-S. Moon, "Measurement noise recommendation for efficient Kalman filtering over a large amount of sensor data," *Sensors*, vol. 19, p. 1168, Mar. 2019.

[21] W. Wang and X. Chen, "Application of improved 5th-cubature Kalman filter in initial strapdown inertial navigation system alignment for large misalignment angles," *Sensors*, vol. 18, no. 2, p. 659, 2018.

[22] B. C. Gao, P. Yang, W. Han, R.-R. Li, and W. J. Wiscombe, "An algorithm using visible and 1.38-μ/m channels to retrieve cirrus cloud reflectances from aircraft and satellite data," *IEEE Trans. Geosci. Remote Sens.*, vol. 40, no. 8, pp. 1659–1668, Aug. 2002.

MIAOMIAO XU was born in China, in 1991. He received the B.E. degree from the Nanjing University of Science and Technology, in 2014, where he is currently pursuing the Ph.D. degree. His research interests are focused on signal process, integrated navigation, and instrumental science and technology.

XIONGZHU BU received the M.E. and Ph.D. degrees in dynamic measurement from the Nanjing University of Science and Technology, Nanjing, in 1990 and 1993, respectively, where he is currently a Professor. His research interests include giant magneto-impedance sensors, dynamic measurements, and digital signal processing.

WEI HAN was born in China, in 1992. He received the B.E. degree from the Nanjing University of Science and Technology, in 2015, where he is currently pursuing the Ph.D. degree in mechanical engineering. His research interests include mechanical design and sensors technology, and dynamic measurements.

YIHAN CAO received the B.E. degree from Jiangsu University, in 2016. He is currently pursuing the Ph.D. degree with the Nanjing University of Science and Technology. His research interests are focused on signal process, integrated navigation, and instrumental science and technology.